frontiers | Frontiers in Marine Science

TYPE Original Research
PUBLISHED 13 January 2026
DOI 10.3389/fmars.2025.1739630

OPEN ACCESS

EDITED BY
Pavel Berloff,
Imperial College London, United Kingdom

REVIEWED BY
Tamay Ozgokmen,
University of Miami, United States
Igor Shevchenko,
University of Southampton, United Kingdom

*CORRESPONDENCE
Eric P. Chassignet
echassignet@fsu.edu

RECEIVED 04 November 2025
REVISED 18 December 2025
ACCEPTED 19 December 2025
PUBLISHED 13 January 2026

CITATION
Chassignet EP and Xu X (2026) Impact of wind stress formulation on Gulf Stream pathway and variability.
Front. Mar. Sci. 12:1739630.
doi: 10.3389/fmars.2025.1739630

Impact of wind stress formulation on Gulf Stream pathway and variability

Eric P. Chassignet* and Xiaobiao Xu

Center for Ocean-Atmospheric Prediction Studies (COAPS), Florida State University, Tallahassee, FL, United States

Current feedback affects surface motions and the numerical experiments presented in this paper highlight its importance when modeling the Gulf Stream. This is not a new notion, but its implementation in the high-resolution 1/50° North and Equatorial Atlantic HYCOM model configuration not only allows us to quantify its impact on the Gulf Stream pathway and variability via detailed comparisons to in-situ and altimetry data, but also to evaluate the latest mean dynamic topography derived from combining altimeter and satellite gravity data, drifters, and hydrological profiles. Introduction of the current feedback induces an "eddy-killing" effect that can reduce the level of eddy kinetic energy (EKE) in the model by as much as 30%, but this drop in EKE can also be compensated by decreasing the model's explicit viscosity accordingly. The current feedback is most effective at damping energy at scales above 50–60 km while the reduction in explicit viscosity leads to an increase in small-scale energy. Addition of the current feedback also does result in a much more realistic distribution of the sea surface height variability and the resulting mean field. The detailed comparison of the model results to altimeter data and *in-situ* measurements leads us to state that the latest mean dynamic topography from CNES-CLS underestimates the maximum Gulf Stream velocity by approximately 10% and that the representation of the shelf circulation may be underestimated.

KEYWORDS

current feedback, eddy kinetic energy (EKE), Gulf Stream, mean dynamic topography, ocean numerical model

1 Introduction

In Chassignet et al. (2023), the authors argued that one not only needs a submesoscale enabled 1/50° grid spacing for a proper representation of the Gulf Stream separation and penetration in basin-scale numerical models (Chassignet and Xu, 2017), but that the inclusion of high-resolution bathymetry, which better resolves the details of the New England seamounts chain (i.e., narrower seamounts and rising higher in the water column), is also required for a more coherent modeled Gulf Stream mean path that better agrees with the observed path. The impact of using high-resolution bathymetry on the modeled Gulf Stream is most striking on the surface variability since it removed an excess of sea surface

height (SSH) variability that is present near the New England seamounts chain (NESC) when using coarse bathymetry. However, while the modeled sea surface variability distribution was significantly improved in the simulation with high-resolution bathymetry when compared to the coarse-resolution bathymetry simulation (Chassignet et al., 2023), a closer look at the sea surface height variability in the high-resolution bathymetry simulation still shows some discrepancies (Figure 1) when compared to altimetry observations, especially south of the mean axis of the Gulf Stream (~38°N) where the model exhibits an excess of variability.

In the quest to have numerical simulations that exhibit surface eddy kinetic energy levels that are comparable to observations, numerical modelers have, until recently, favored using absolute wind stress in the atmospheric forcing formulation since it is well documented that computing the wind stress using winds relative to the ocean current damps mesoscale ocean motions and reduces the surface kinetic energy by approximately 25 to 30% (Dewar and Flierl, 1987; Jullien et al., 2020). The impact is quite severe on the ocean interior when the grid spacing is on the order of 1/10° or larger and when eddy motions are limited by the viscosity required to keep the model numerically stable (Chassignet et al., 2020). There are, however, localized benefits to using relative winds such as improved representations of the Gulf Stream and Agulhas Retroflection paths and associated eddy activity in regional numerical models (Renault et al., 2016, 2017; Larrañaga et al., 2022) as well as in global numerical models (Chassignet et al., 2020). For example, integration of ocean surface currents into the ocean–atmosphere coupling interface of the Regional Oceanic Modeling System (ROMS) was shown by Renault et al. (2016) to stabilize the Gulf Stream separation and postseparation, resolving long-lasting biases in previous ROMS modeled Gulf Stream paths. These biases in Gulf Stream separation and pathway, however, are not universal across numerical models, e.g., the Gulf Stream separation in HYCOM (HYbrid Coordinate Ocean Model; Bleck, 2002) and its predecessor MICOM (Miami Isopycnic Coordinate Model; Bleck and Chassignet, 1994) has always been stable and reasonably well represented as long as the solution is inertial enough (1/12° or finer grid spacing) (Paiva et al., 1999; Chassignet and Garraffo, 2001; Chassignet and Marshall, 2008; Hurlburt et al., 2011; Chassignet and Xu, 2017).

As elegantly stated by Samelson et al. (2024), the inclusion of the ocean current in the relative wind formulation means that, in effect, "the air–sea interface acts in the long-term mean like a rigid boundary with a no-slip condition on the ocean flow and a drag coefficient that depends on wind speed". In other words, this "top drag" (Dewar and Flierl, 1987) damps mesoscale activity [i.e. "eddy killing" as defined by Renault et al. (2016)] and is a sink of energy that can be comparable or greater than bottom drag or viscosity. As shown in Figure 1, there is an excess of variability remaining in the North and Equatorial HYCOM 1/50° of Chassignet et al. (2023) and this raises the question as to whether this could be a consequence of using absolute winds instead of relative winds as preconized by Renault et al. (2020) and others. Jullien et al. (2020) argue that, by not considering the current feedback on the atmosphere and neglecting its impact, this artificially increases the insufficient EKE, but for the wrong reasons, relying too much on numerical dissipation and explicit viscosity to keep the solution in line with the observations.

In this paper, we indeed show that the inclusion of ocean-atmospheric feedback not only removes the excess SSH variability shown in Figure 1, but also further improves the Gulf Stream mean path as surmised by Renault et al. (2016). A detailed comparison to *in-situ* observations (Oleander and W lines) quantifies the improvement and also leads us to state that the current mean dynamic topography (MDT) used in altimetry (Jousset et al., 2025) underestimates the strength of the Gulf Stream around 70°W by approximately 10%.

The layout of the paper is as follows. Section 2 describes the model configuration and forcing. Section 3 quantifies the impact of the ocean-atmospheric feedback on the Gulf Stream pathway and variability and the model results are compared in detail to *in-situ* measurements along the Oleander and W lines. Power spectra are also used to document the impact of replacing viscosity as the energy sink by the ocean-atmospheric feedback eddy killing on small scale motions. Finally, the results are summarized and discussed in Section 4.

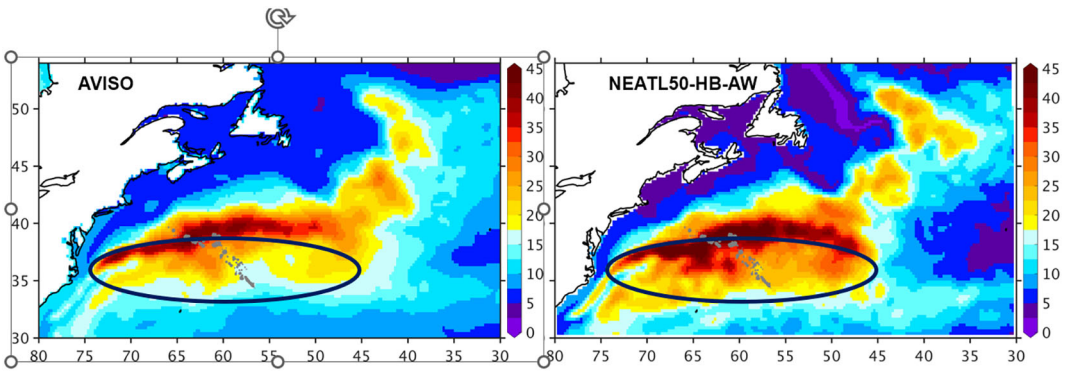

FIGURE 1
SSH root mean square (RMS) for the gridded AVISO sea level anomaly derived from altimetry (1993-2022) and the high-resolution bathymetry absolute wind experiment (NEATL50-HB-AW, 5-year mean).

2 Model configuration and atmospheric forcing

The HYbrid Coordinate Ocean Model (HYCOM) configuration used in this paper is identical to that of Chassignet and Xu (2017) and of Chassignet et al. (2023) and covers the North Atlantic from 28°S to 80°N [see Figure 1 of Chassignet and Xu (2017)]. In this paper, we analyze three 1/50°configurations (2.25 km at the equator, 1.5 km in the Gulf Stream region), which differ in bathymetry and atmospheric forcing formulation (Table 1) as well as in viscosity (Table 2). The coarse-resolution (CB) model bathymetry, used in the reference North and Equatorial Atlantic experiment of Chassignet and Xu (2017), hereafter referred to as NEATL50-CB-AW, is linearly interpolated from a coarser 1/12° bathymetry based on the 2' Naval Research Laboratory (NRL) digital bathymetry database, which combines the global topography based on satellite altimetry of Smith and Sandwell (1997) with several high-resolution regional databases. The bathymetry for the high-resolution bathymetry (HB) experiments NEATL50-HB-AW and NEATL50-HB-RW, on the other hand, is derived from the latest 15 arc-seconds GEBCO bathymetry (https://www.gebco.net/data_and_products/gridded_bathymetry_data/) and therefore contains significantly higher resolution topographic features [Figures 1 and 2 of Chassignet et al. (2023)].

In the vertical, the simulation contains 32 hybrid layers with density referenced to 2000 m (σ_2) (see Chassignet and Xu (2017) for details). The vertical coordinate in HYCOM (Bleck, 2002) is isopycnal in the stratified open ocean and makes a dynamically smooth and time dependent transition to terrain-following in shallow coastal regions and to fixed pressure levels in the surface mixed layer and/or unstratified seas (Chassignet et al., 2003, 2006). No inflow or outflow is prescribed at the northern and southern boundaries. Within a buffer zone of about 3° from the northern and southern boundaries, the 3-D model temperature, salinity, and depth of isopycnal interface are restored to the monthly Generalized Digital Environmental Model (GDEM) (Teague et al., 1990; Carnes, 2009) climatology with an e-folding time of 5–60 days that increases with distance from the boundary. The reference configuration NEATL50-CB-AW is initialized using potential temperature and salinity from the GDEM climatology and spun-up from rest for 20 years. Both NEATL50-HB-AW and NEATL50-HB-RW were initialized from the end of year 15 of NEATL50-CB-AW and integrated for 5 years.

TABLE 1 North and Equatorial Atlantic model configurations.

1/50° experiment (Δx ~ 1.5 km)	Bathymetry	Forcing
NEATL50-CB-AW	2' Naval Research Laboratory (Δx ~ 2.5 km)	Absolute Wind
NEATL50-HB-AW	15 arc-seconds GEBCO (Δx ~ 300 m)	Absolute Wind
NEATL50-HB-RW	Same as NEATL-HB-AW	Relative Wind 70%

TABLE 2 Viscosity and diffusion coefficients.

Parameters	NEATL50-CB-AW	NEATL50-HB-AW	NEATL50-HB-RW
Laplacian coefficient for momentum	10 m^2/s	10 m^2/s	5 m^2/s
Biharmonic diffusive velocity (V_4) for momentum	4 cm/s	4 cm/s	1 cm/s
Biharmonic diffusive velocity for layer thickness	4 cm/s	4 cm/s	1 cm/s
Laplacian diffusive velocity for tracers	1 cm/s	1 cm/s	0.5 cm/s

The three numerical experiments use the same climatological atmospheric forcing from the ECMWF reanalysis ERA40 (Uppala et al., 2005) with 3-hourly wind anomalies from the Fleet Numerical Meteorology and Oceanography Center (FNMOC) 3 hourly Navy Operational Global Atmospheric Prediction System (NOGAPS) for the year 2003. The year 2003 is considered a neutral year over the 1993-present timeframe in terms of long-term atmospheric patterns, such as the North Atlantic Oscillation. The difference between the absolute wind (AW) and relative wind (RW) experiments is in the formulation of the wind stress. As stated by Renault et al. (2020), in a fully coupled ocean-atmosphere environment, the wind stress is computed using the wind relative to the oceanic current, which varies in time and provides an ocean current feedback to the atmosphere. Coupled simulations are, however, expensive and ocean-only simulations are usually forced by a prescribed atmospheric reanalysis. The question then arises as to what is the best way to force an ocean-only numerical model and still take into account the current feedback to the atmosphere. Renault et al. (2020) in their "recipes for how to force an oceanic model" suggest using in the bulk formula $\tau = \rho C_D \mathbf{U_r}|\mathbf{U_r}|$ where $\boldsymbol{\tau}$ is the surface stress, is the air density, and $\mathbf{U_r}$ is the wind relative to the oceanic motion defined as $\mathbf{U_r} = \mathbf{U_a} - (1 - s_w)\mathbf{U_o}$. $\mathbf{U_a}$ is the atmospheric wind at 10 m, $\mathbf{U_o}$ is the oceanic current, and s_w corresponds to the linear wind response to a given current and is a correction coefficient parameterizing the current-wind coupling. If the wind cannot feel the surface oceanic current, then $s_w = 0$, there is no wind response to the current. If $s_w = 1$, there is no loss of energy, the current generates a wind with a magnitude equal to the current magnitude which corresponds to the stress used in the absolute wind (AW) forcing cases (see Renault et al., 2020 for details). Based on a series of coupled experiments, Renault et al. (2020) suggest using a constant $s_w = 0.3$ to take into account the current feedback to the atmosphere (equivalent to using 70% of the ocean velocity in the stress formulation) and this is what we use in our relative wind (RW) experiment. One can also use monthly and spatial variations of s_w or another simple parameterization based on a current stress-coupling coefficient s_T. Although all the parameterizations led to relatively similar results, Renault et al. (2020) recommends the parametrization using predicted s_T for its flexibility on a global scale. We however decided to use a constant $s_w = 0.3$ as it is not dependent on any s_T derivation.

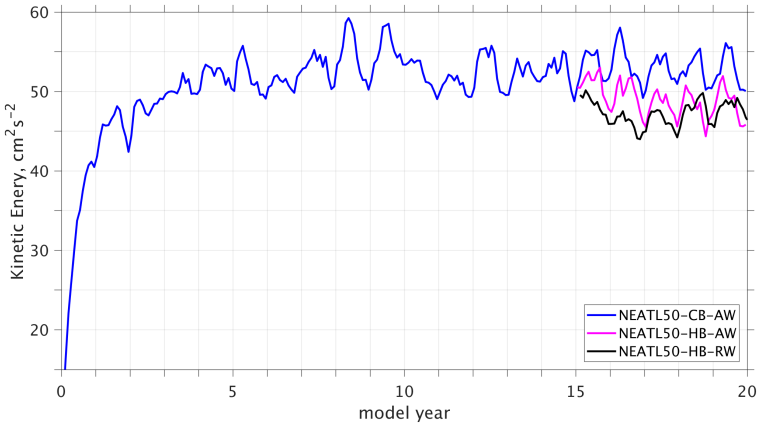

FIGURE 2
Basin average kinetic energy for the three numerical simulations: NEATL50-CB-AW, NEATL50-HB-AW, and NEATL50-HB-RW. Units are in cm^2/s^2.

The viscosity and diffusion parameters for all experiments are listed in Table 2. The horizontal viscosity operator is a combination of Laplacian ($A_2 = \max(0.5\Delta x^2$ times the Smagorinsky deformation tensor, A) and bihamonic ($A_4 = V_4\Delta x^3$). The values for the coefficients in the 1/50° of Chassignet and Xu (2017) were kept close to that of the 1/25° in order to isolate the impact of resolving the submesoscale on the solution. As stated in the introduction, when relative wind forcing is prescribed, one anticipates a decrease in the order of 25 to 30% in basin-wide kinetic energy. One can, however, adjust for this loss of energy by reducing the magnitude of the viscosity and diffusivity coefficients and making the solution less dependent on the subgrid scale parameterizations. The decreases in the viscosity and diffusivity coefficients of NEATL50-HB- RW (relative wind) when compared to that of NEATL50-HB-AW (absolute wind) are summarized in Table 2. The K-profile parameterization of Large et al. (1994) is used for vertical mixing in the surface mixed layer as well as in the ocean interior. The bottom drag is quadratic with a coefficient of 10^{-3} and a background RMS flow speed of $5x10^{-2}$ m/s.

The basin kinetic energies for experiments NEATL50-HB-AW and NEATL50-HB-RW adjust quickly in less than a year (Figure 2) after being initialized from year 15 of NEATL50-CB-AW. In the high-resolution bathymetry NEATL50-HB-AW, the basin kinetic energy is approximately 10% lower than in its coarse-resolution counterpart NEATL50-CB-AW, presumably because of the increased form drag and increased Reynolds stresses induced by the more refined bathymetry (Davis et al., 2025). Despite the use of relative winds in NEATL50-HB-RW, the kinetic energy is at the same level as NEATL50-HB-AW after five years. This is because the reduced viscosity and diffusivity in NEATL50-HB-RW (Table 2) compensates for the sink of energy induced via eddy killing. The comparable sink of energy is achieved via higher explicit viscosity/dissipation in NEATL50-HB-AW (see Jullien et al. (2020) for a discussion).

3 Impact of relative versus absolute wind forcing on Gulf Stream pathway and variability

3.1 Sea surface height variability

The fact that we first ensured that the basin-wide kinetic energy is at the same level in both the AW and RW simulations (section 2) allows us to compare the surface fields on an equal footing knowing that any differences are due to a redistribution of the sources and sinks of energy. Figure 3 displays the SSH variability for NEATL50-HB-RW and NEATL50-HB-AW in comparison to AVISO. As surmised by Renault et al. (2016) and extensively discussed in more recent publications (Jullien et al., 2020; Samelson et al., 2024), inclusion of the relative wind/current feedback in NEATL50-HB-RW leads to a spatial distribution of the SSH RMS that is in much better agreement with AVISO than its absolute wind counterpart (NEATL50-HB-AW). As highlighted by the difference plots, much of the absolute wind experiment excessive SSH variability present in the Gulf Stream and vicinity (Figure 3e) is removed or significantly reduced in the relative wind experiment (Figure 3f) and the 25 cm SSH RMS contour in the relative wind experiment essentially overlaps that of the AVISO observations (Figure 3d).

The improvement in SSH variability, as shown in Figures 3c, e, can be further quantified by displaying the zonally averaged SSH RMS between 47.5°W and 72.5°W as a function of latitude and the meridionally averaged SSH RMS between 35°N and 42.5°N as a function of longitude for the two numerical experiments and AVISO. Meridionally (Figure 4a), there is clearly an excess of SSH RMS south of about 39°N in the absolute wind experiment when compared to the observed AVISO product. With the introduction of relative wind, this excess of SSH RMS is significantly reduced and the SSH RMS distribution spatially

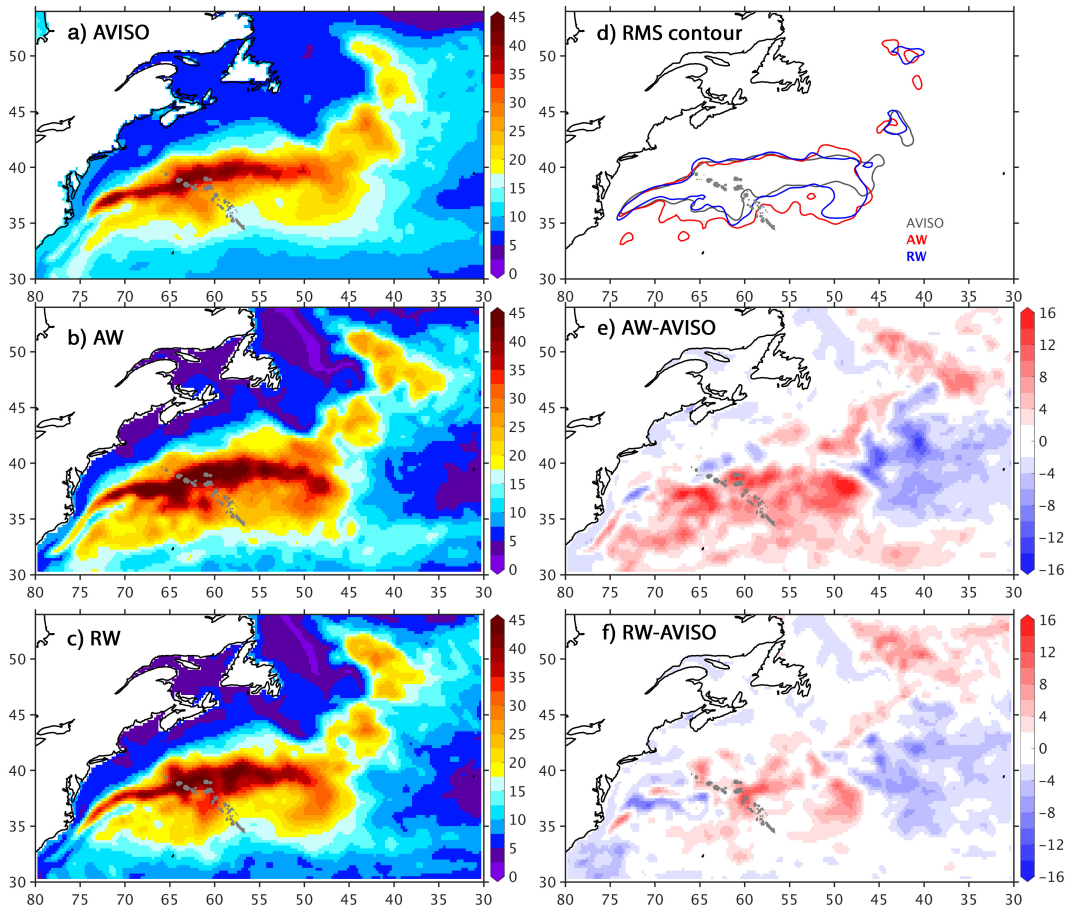

FIGURE 3
SSH RMS for AVISO (1993-2022), NEATL50-HB-RW, and NEATL50-HB-AW **(a–c)**. The 25 cm RMS contours are shown in panel **(d)** and the differences from the AVISO fields are shown in panels **(e, f)**. The model fields (5-year mean) are filtered to match the AVISO processing (i.e., 15-day and 150-km low pass) as described in Chassignet and Xu (2017).

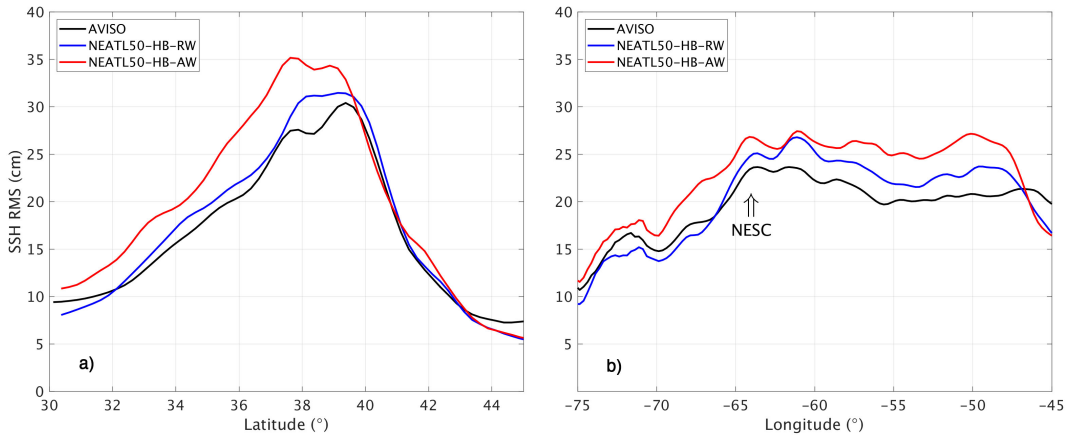

FIGURE 4
(a) Zonally averaged SSH RMS (in cm) between 47.5°W and 72.5°W as a function of latitude and **(b)** meridionally averaged SSH RMS (in cm) between 35°N and 42.5°N as a function of longitude.

matches the observations (Figure 3e). Zonally (Figure 4b), the reduction in SSH RMS in relative wind experiment takes place both upstream and downstream of the NESC. Another measure to quantify the improvement is to compute the zonally averaged SSH RMS as a function of the distance (in km) from the main axis of the Gulf Stream (i.e., stream-coordinate). The main Gulf Stream axis is defined as the maximum SSH RMS at a given longitude (see Figure 5a for AVISO as an example). The width over which the SSH variability extends north and south of the main path is reduced everywhere in the relative wind experiment (Figure 5b). The differences between Figure 4a and Figure 5b reflect the fact that the main Gulf Stream axis is not exactly zonal from 72.5°W to 47.5°W.

3.2 Mean SSH and velocities

The mean SSH fields are displayed in Figures 6a–c for the numerical simulations NEATL50-HB-AW and NEATL50-HB-RW and for the best observed CNES-CLS22 estimate (derived from combining altimeter and satellite gravity data, drifters, and hydrological profiles; see Jousset et al. (2025) for details). At first glance, they all look quite similar, but there are some significant differences. Specifically, in the absolute wind experiment (NEATL50-HB-AW), the inertial gyre south of the Gulf Stream before the NESC extends too far south and west when compared to the observations and to the relative wind experiment. This extended inertial gyre is the signature of a rectified flow resulting from the excess of eddy variability in the region (i.e. cold core eddies – see Figure 3e). The mean SSH contours are also more spread out downstream of the NESC in NEATL50-HB-AW when compared to NEATL50-HB-RW and CNES-CLS22, again from an excess of variability south of the main axis of the Gulf Stream as shown in Figure 3. This is better illustrated in Figure 6d which shows the time-averaged SSH contours corresponding to the location for the northern (-25 cm) and southern (50 cm) edge of the Gulf Stream. On average, the SSH southern contour extends significantly further east in NEATL50-HB-AW than in NEATL50-HB-RW and CNES-CLS22. Overall, excessive SSH variability leads to a wider mean Gulf Stream recirculating gyres both upstream and downstream of the NESC in the absolute wind experiment. In the relative wind experiment (NEATL50-HB-RW), less variability leads to a more coherent and tighter jet which is better agreement with the observations (Figures 6e, f), especially east of the NESC.

One can further quantify the differences in mean SSH (Figures 6e, f) by comparing the zonally averaged mean SSH between 47.5°W and 72.5°W as a function of latitude (Figure 7a). South of the Gulf Stream main axis, the excess of SSH variability in the absolute wind experiment (Figure 3e) leads to a significantly higher SSH when compared to the CNES-CLS22 MDT. North of the Gulf Stream main axis, the two numerical simulations agree with each other, but both differ substantially from the CNES-CLS22 MDT. The negative SSH slope extends north of 40°N in the numerical simulations and the Gulf Stream's width is wider on average than in the CNES-CLS22 estimate. Also, north of 40°N, the observations-based CNES-CLS22 MDT shows almost no gradient in the SSH contours (Figure 6a). This either implies that the representation of the shelf circulation is incorrect in the models or that there are not enough observations to ensure a proper derivation of an observed mean for that region. Chen and Yang (2024) report a similar finding as their high-resolution model also captures additional features that are missing from the CNES-CLS22 MDT, including the Labrador coastal current and a shelf break jet off the continental shelf of the US northeast, currents that have been verified in previous studies (e.g., Lazier and Wright, 1993; Loder et al., 1998). A similar picture (Figure 7b) arises when the mean SSH profile is computed as a function of the distance (in km) from the main axis of the Gulf Stream (defined as for the SSH RMS), but there is a clearer contrast between NEATL50-HB-AW and NEATL50-HB-RW, with the SSH mean of the relative wind experiment being again closer to the observed mean than the absolute wind experiment. The SSH slope is also significantly steeper in the stream-coordinate averaged mean (Figure 7b) than in the Eulerian average (Figure 7a) since the core strength of the jet is retained when doing the average (Figure 7b).

The distributions of the geostrophic velocity $\mathbf{v} = (-\frac{1}{f}\frac{\partial \eta}{\partial y}, \frac{1}{f}\frac{\partial \eta}{\partial x})$ (Figures 7c, d) mirror the SSH since the magnitude of the velocity is directly related to the SSH slope (η is the sea surface height and f,

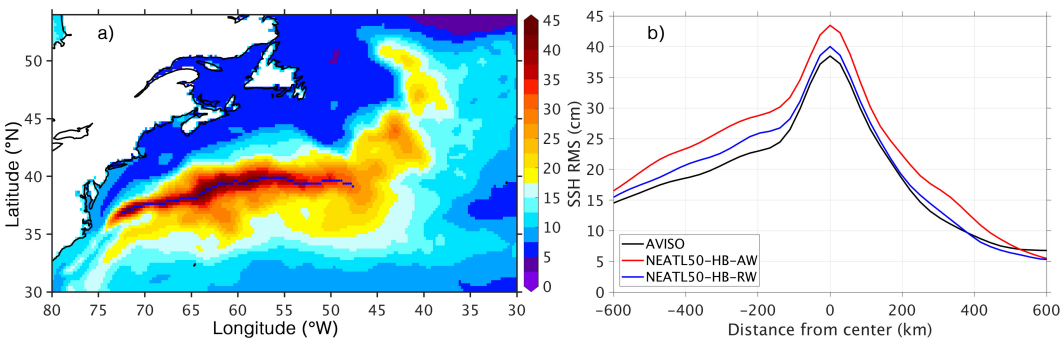

FIGURE 5
(a) Location of the maximum SSH RMS for AVISO (1993-2022) and **(b)** zonally averaged SSH RMS (in cm) as a function of the distance from the main axis of the Gulf Stream (in km; negative is south, positive is north) defined as the maximum SSH RMS (AVISO, NEATL50-HB-RW, and NEATL50-HB-AW, respectively) at a given longitude (see left panel as example for AVISO).

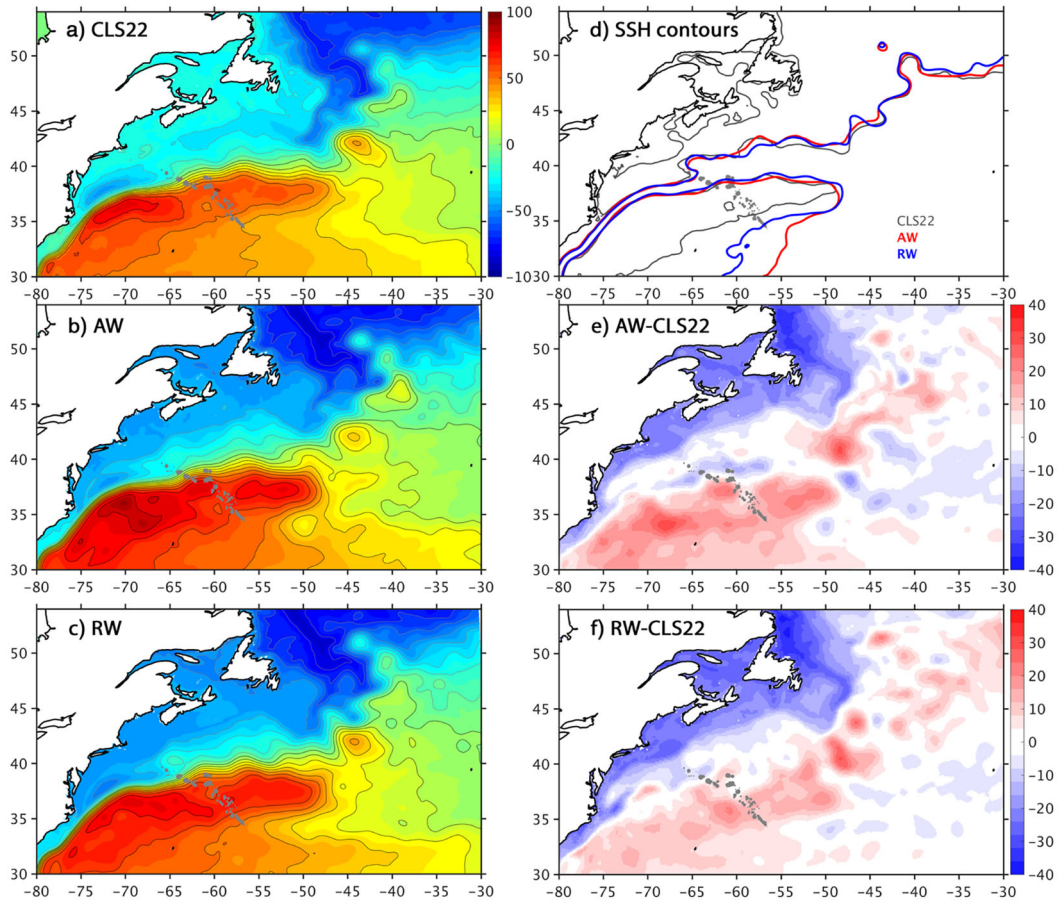

FIGURE 6
(a, b) 5-year mean SSH fields for NEATL50-HB-AW and NEATL50-HB-RW, **(c)** CNES-CLS22 (Jousset et al., 2025); **(d)** time-averaged SSH contours showing the location for the northern (-25 cm) and southern (50 cm) edge of the Gulf Stream in the northwestern North Atlantic for CNES-CLS22 (grey), NEATL50-HB-AW (red), and NEATL-HB-RW (blue). The location of NESC is indicated by a series of small, closed grey contours between 68° and 57°W; **(e, f)**. differences between CNES-CLS2 and NEATL50-HB-AW/NEATL50-HB-RW mean SSH fields, respectively.

the Coriolis parameter). But small differences in mean SSH slope that cannot be distinguished in Figures 6a–c and Figures 7a, b become explicit when computing its derivative. In Figure 7c (Eulerian average), one can note that there are two maxima in the velocities in both CNES-CLS22 and NEATL50-HB-RW, but not in NEATL50-HB-AW, again illustrating how using relative winds increases the realism of the numerical solution. Both numerical experiments show higher velocities than the ones derived from the CNES-CLS22 MDT, both zonally (Figures 7c, d) and meridionally (Figure 8). One can further quantify the differences in core velocities by computing the zonal average of the along stream-coordinate geostrophic velocities as in Halkin and Rossby (1985) (Figure 7d). We find that the CNES-CLS22 derived maximum Gulf Strem velocities are 25% weaker than in the numerical experiments and the question then arises as to whether the numerical solutions are too energetic or if the CNES-CLS22 underestimates the observed SSH gradient. This is addressed in the following subsection by comparing the numerical model to *in-situ* velocity measurements along the Oleander and W lines.

3.3 Comparison with the Oleander and W lines

As stated in the previous section, the Gulf Stream maximum geostrophic mean velocity in the numerical models is larger than those derived from the CNES-CLS MDTs (Figures 7, 8). The CNES-CLS MDTs are generated by combining altimeter and satellite gravity data, drifters, and hydrological profiles and those estimates have been routinely updated over the years (Rio and Hernandez, 2004; Rio et al., 2011, 2014; Mulet et al., 2021; Jousset et al., 2025). There is significant variability among these observations-based MDTs (2009, 2013, 2018, and 2022) with the latest 2022 MDT having the largest Gulf Stream maximum mean velocity (see Figures 7, 8). In this section, we use *in-situ* measurements to quantify the accuracy of the CNES-CLS22 MDT climatology and further assess the realism of the numerical simulations. The measurements are time-averaged Gulf Stream velocity, property structures and transport estimates constructed by Rossby et al. (2019) and Andres et al. (2020) using sections of

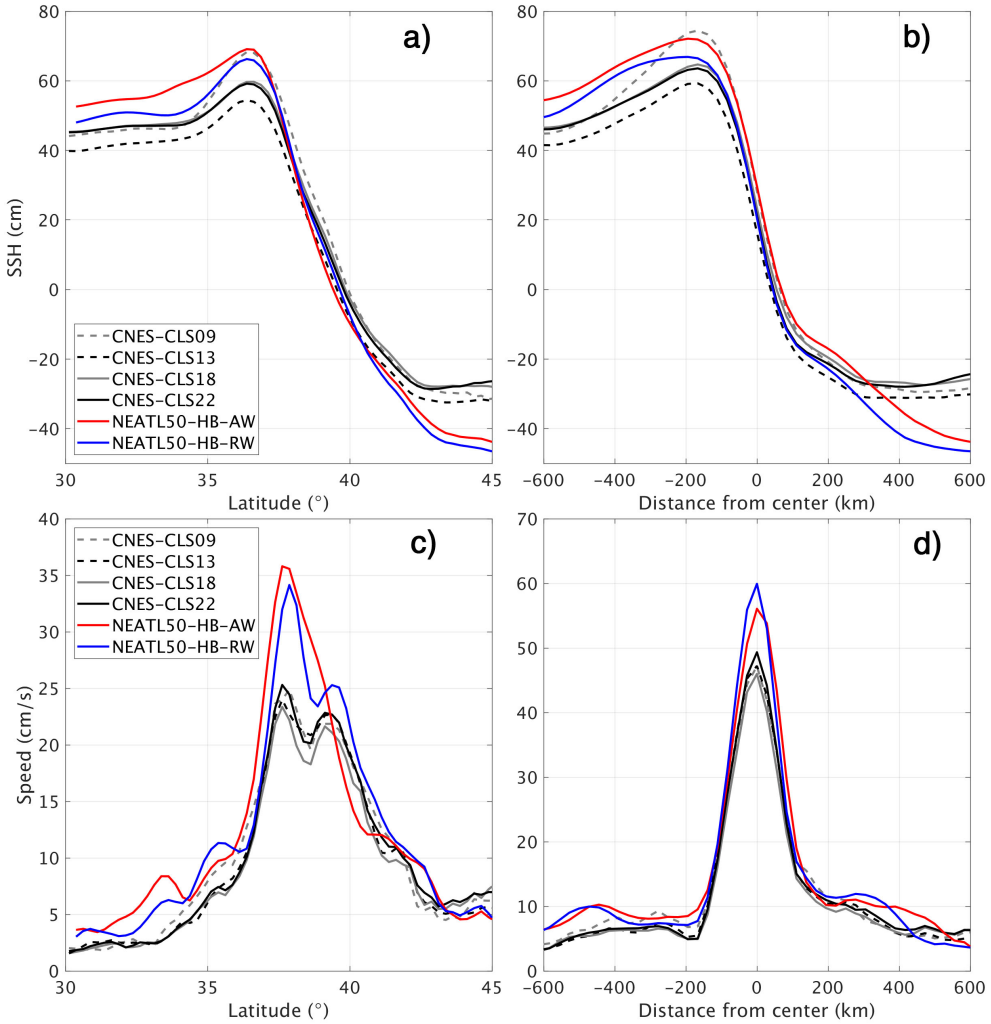

FIGURE 7
(a) Zonally averaged SSH, **(b)** zonally averaged stream-coordinate SSH, **(c)** zonally averaged geostrophic velocity, and **(d)** zonally averaged stream-coordinate geostrophic velocity for the CNES-CLS means (2009, 2013, 2018, and 2022) and for NEATL50-HB-AW and NEATL50-HB-RW. The zonal average is between 47.5°W and 72.5°W.

full-ocean-depth observations of horizontal velocity, temperature, and salinity taken during 2005–2018 along the Oleander line (70.3° W) and the W line (68.5°W) (see Figure 9 for locations of the lines and stations).

The mean surface geostrophic velocity and their respective differences are shown in Figure 9 for CNES-CLS22, NEATL50-HB-AW, and NEATL50-HB-RW. The modeled velocities are larger on average and the core velocity in the relative wind experiment extends further east than in the absolute wind experiment. Both numerical experiments show a remarkable agreement with the observations in the Gulf Stream pathway and separation. For reference and before looking at the *in-situ* measurements, we first compare the modeled SSH time-mean, surface geostrophic velocities, and SSH variability along the Oleander and W lines to those derived from CNES-CLS22 and AVISO, respectively (Figure 10). The SSH changes across the Gulf Stream in the models are comparable to the latest CNES-CLS MDTs. The earlier CNES-CLS09 is an outlier as discussed by Worst et al. (2014). The mean model velocities normal to the Oleander and W lines are indeed larger than the ones derived from the observations, either as Eulerian (Figure 10) or stream-coordinate (Figures 11, 12) averages. In all cases (numerical simulations and CNES-CLS22), there is a significant drop (~20 cm/s) in the maximum Eulerian mean velocities from the upstream Oleander line to the downstream W line (Figure 9), but this drop is more pronounced in NEATL50-HB-AW (Figures 9, 10). However, when the mean velocity is computed using the stream-coordinate velocities (Figures 12a, b), there is very little difference in the core strength of the Gulf Stream between NEATL50-HB-AW and NEATL50-HB-RW and the velocity drop from Oleander to W is significantly smaller. This implies that the larger decrease in the absolute wind NEATL50-HB-AW experiment of the Eulerian Gulf Stream mean velocities at the W line, when compared to the Oleander line, is a consequence of its higher downstream eddy variability (Figures 10e, f). The downstream eddy variability is significantly smaller in NEATL50-HB-RW and is comparable to

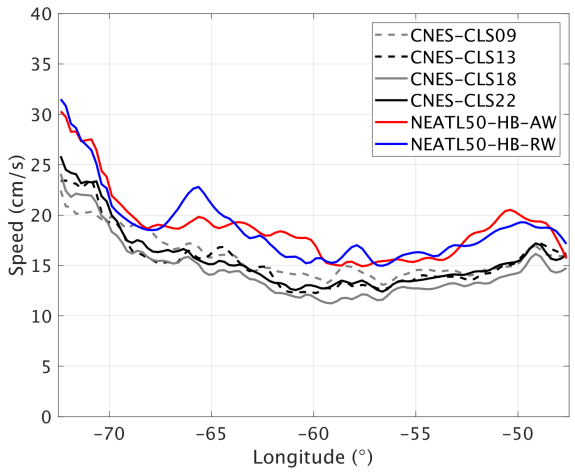

FIGURE 8
Meridionally averaged geostrophic velocities between 35°N to 42.5° N for the CNES-CLS means (2009, 2013, 2018, and 2022) and for NEATL50-HB-AW and NEATL50-HB-RW.

AVISO (Figures 10e, f). Also, we note that neither AVISO nor the models show the significant decrease (~40 cm/s) in the Gulf Stream core stream-averaged velocities from the Oleander section to the W section (see Figure 12) that was reported by Andres et al. (2020).

We now compare the model velocities to the *in-situ* measurements at the Oleander and W lines (Rossby et al., 2019; Andres et al., 2020; Rossby et al., 2025) (Figures 12, 13) to address the following: Are the lower AVISO-derived velocities due to an underestimation of the MDT by CNES-CLS22 or are the model results too energetic? Why is the decrease (~40 cm/s) in the Gulf Stream core stream-averaged velocities from the Oleander section to the W section reported by Andres et al. (2020) not seen in the numerical models (NEATL50-HB-AW/NEATL50-HB-RW), nor in the altimetry (AVISO/CNES-CLS22)?

Along the Oleander line, SADCP measurements have been collected since 1992 and a set of near 500 complete, quasi-synoptic occupations of the Gulf Stream during 2005-2018 (Rossby et al., 2019) were processed to generate the upper-ocean velocity in stream coordinates from near surface (55 m) to 700 m depth, at ~3 km horizontal (across stream) and 25–50 m vertical

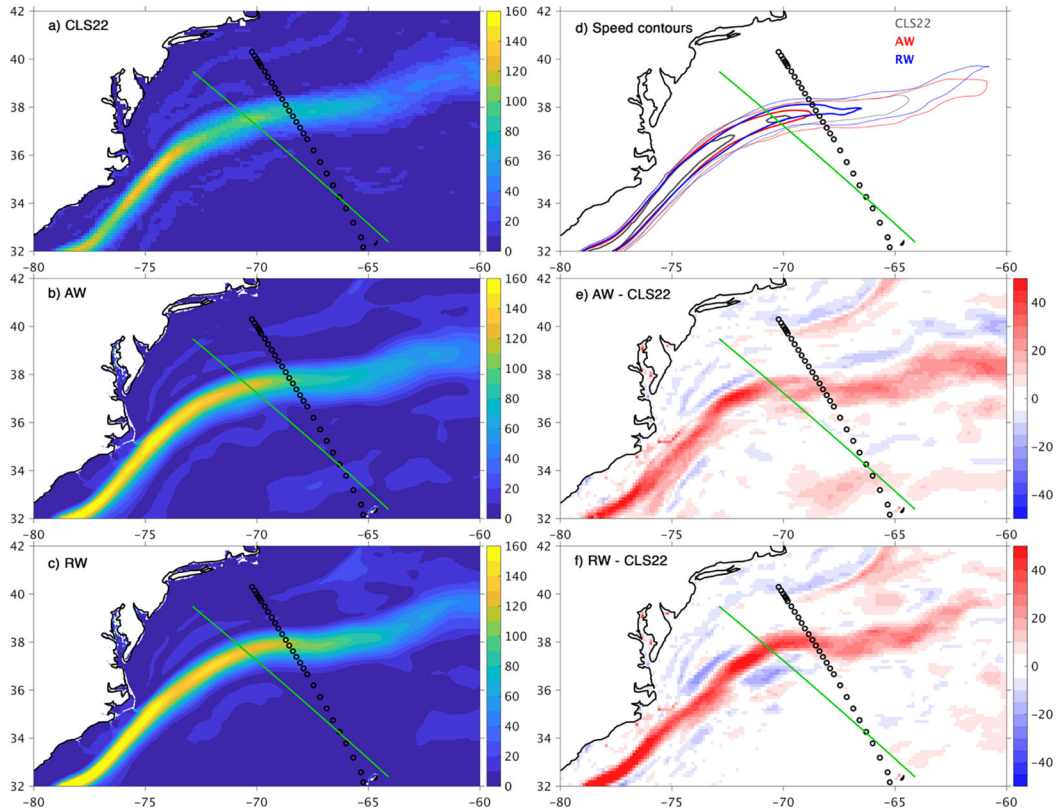

FIGURE 9
Mean surface geostrophic speed for **(a)** CNES-CLS22, **(b)** NEATL50-HB-AW, and **(c)** NEATL50-HB-RW. The velocity contours in d) are 1 m/s (thick lines) and 50 cm/s (thin lines). The velocity differences with CNES-CLS22 are shown in **(e, f)** for NEATL50-HB-AW and NEATL50-HB-RW, respectively. The green line is the Oleander section and the black circles are the line W stations.

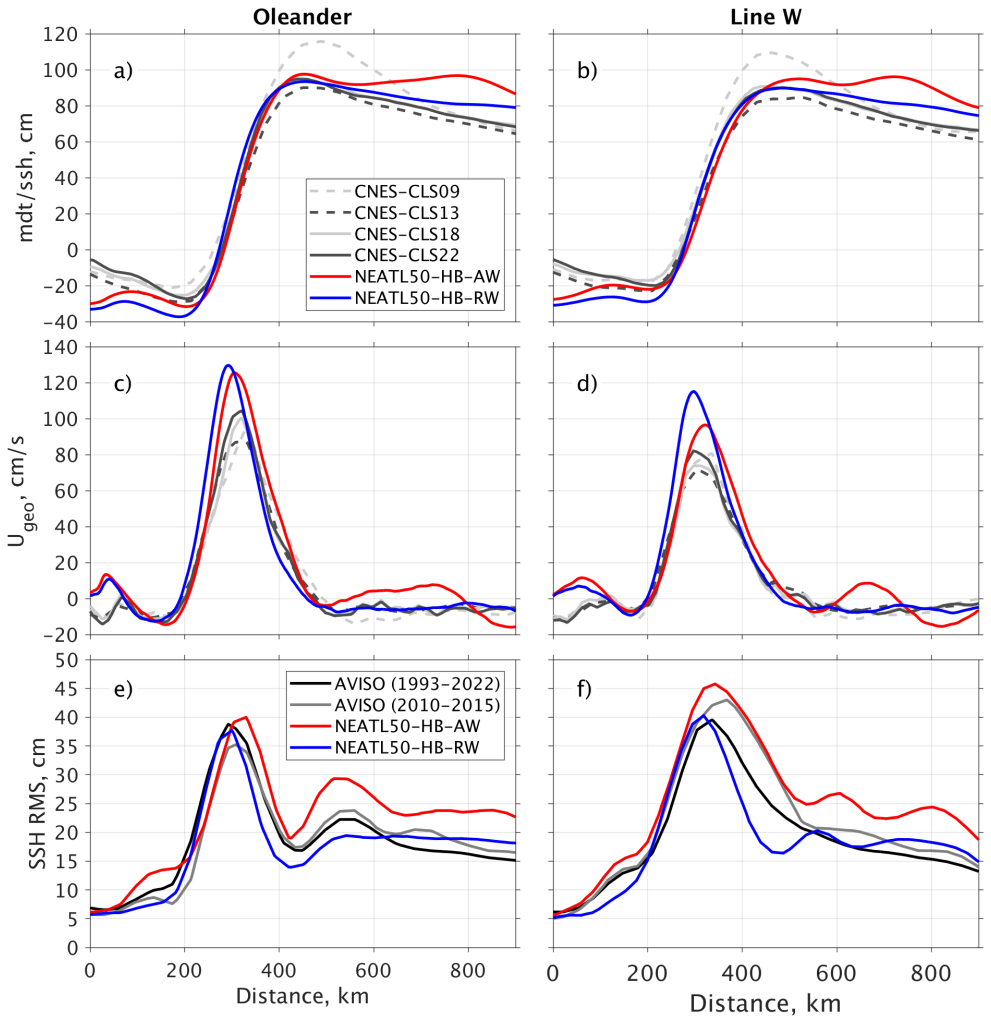

FIGURE 10
Eulerian time mean SSH **(a, b)**, surface geostrophic velocity **(c, d)**, and SSH RMS **(e, f)** along the Oleander and W lines

resolution. The time averages (Eulerian and stream average) of these sections are shown in Figure 13 for the SADCP measurements and for the two model simulations. The location and strength of the Gulf Stream core along the Oleander line are well represented in the model simulations (Figure 13), but it is more surface intensified in HYCOM with velocities at 55 m (first level where the observations can be mapped) being stronger than the observations by 15 to 20 cm/s in the Eulerian mean and 20–25 cm/s in the stream-averaged mean (Figures 11c, d). In both the Eulerian and stream-averaged mean, the model Oleander velocities are in line with the observations at 505 m (Figures 11, 13).

When comparing *in-situ* velocities to velocities at the surface derived from AVISO, one needs to take into account the fact that AVISO velocities are geostrophically derived from the SSH fields and that the AVISO SSH anomalies are heavily filtered in space and time (Chassignet and Xu, 2017). The difference between geostrophic and total velocities is on average quite small (less than 5 cm/s) in the two model simulations (Figures 11a, b). The time and space filtering, on the other hand, significantly reduces the maximum Gulf Stream modeled peak velocities (Figure 11b) by ~50 cm/s and makes the jet wider, especially on the northern side of the Gulf Stream axis. The AVISO peak and filtered modeled velocities therefore differ by ~40 cm/s. This difference is due (a) a stronger jet in the model (~25/30 cm/s) as shown above and (b) an underestimation of the CLS-CNES22 mean peak velocity of ~10–15 cm/s.

Here is how we arrived at the conclusion that there is indeed an underestimation of the maximum geostrophic velocity when derived from the CNES-CLS22 MDT together with an overestimation of the maximum velocity by the numerical models. First, we estimate that, at the Oleander section, the maximum observed Eulerian averaged Gulf Stream speed at the surface is ~1.15 m/s, given that the Oleander-measured maximum velocity is 1.10 m/s at 55 m and that the difference in velocities seen in the model between the surface and 55 m is ~5 cm/s in the Eulerian mean (Figure 11). Taking into account that there is also a ~5 cm/s difference between full velocities and geostrophic velocities (as computed from the numerical simulations – see Figure 14a), we

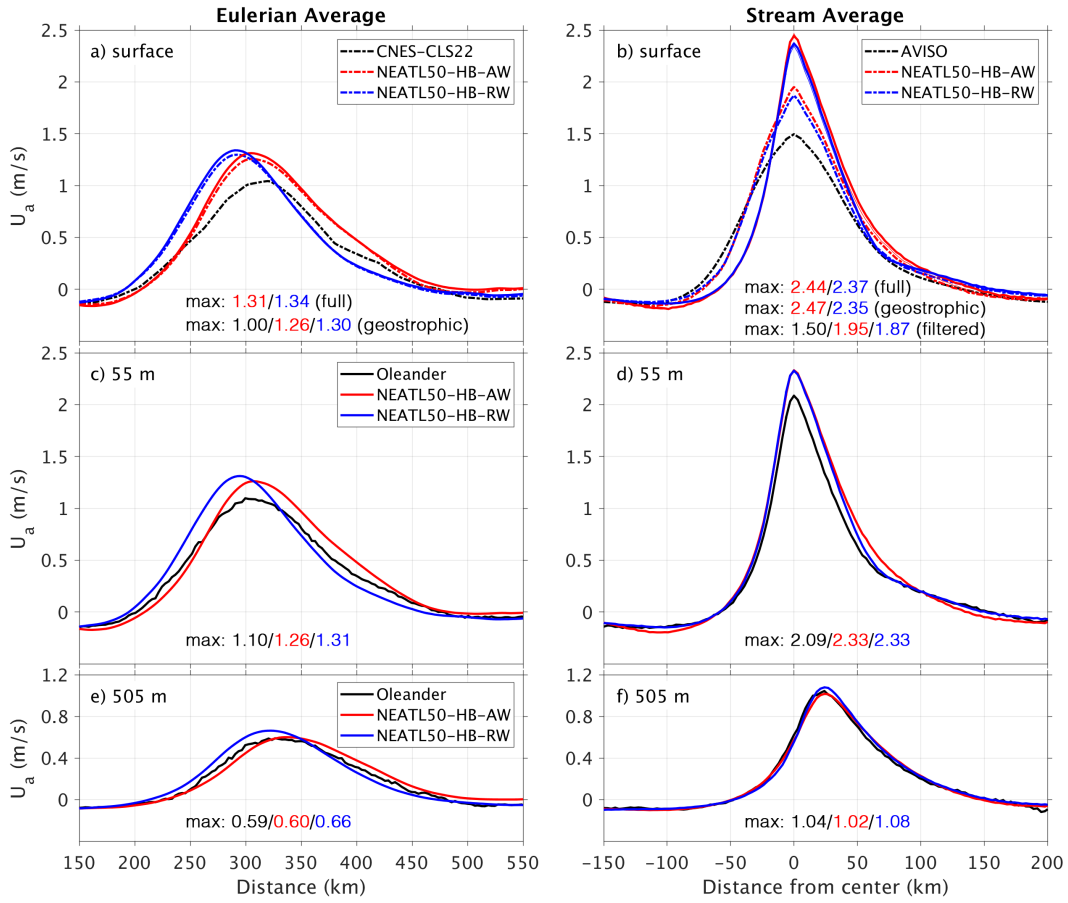

FIGURE 11
A comparison of the Gulf Stream between Eulerian and stream average along the Oleander line at **(a, b)** surface, **(c, d)** 55 m, and **(e, f)** 505 m. In all panels, solid thick lines are total unfiltered velocities. In panel **(a)**, the dash doted lines are geostrophic velocities and in **(b)**, the dash doted lines are geostrophic velocities filtered to match the AVISO processing (i.e., 15-day and 150-km low pass) – geostrophic velocities cannot be distinguished from full velocities (see Figure 12).

need to reduce by the above estimate by ~5 cm/s to arrive to a number that can be compared to the surface geostrophic velocity derived from the CNES-CLS22 mean SSH of ~1.00 m/s. The difference is 10 cm/s and this therefore implies an underestimation of the maximum Eulerian mean speed by CNES-CLS22 by approximately 10%.

Andres et al. (2020) using 2010–2014 observations along the Oleander and W sections reported a significant drop (~40 cm/s or 25%), in the maximum of the along stream core velocity from the Oleander to the W line at 77 m depth (Figures 12c, d). This large drop is not present in the model simulations, nor is it consistent with surface measurements derived from AVISO (Figures 12a, b). AVISO shows only a small decrease (~5%) in the maximum surface core velocity when compared to the 25% decrease at 77 m depth derived from the combined SADCP, LADCP, and moorings measurements. Not only is the decrease in the modeled core velocities (surface and 77 m) between the two sections consistent with the AVISO, the model and the observed velocities also do not show any significant decrease at 500 and 1000 m between the two sections and agree with each other. The LADCP measurements do, however, appear to systematically provide velocities that are lower than the velocities derived from the moorings' records (Figure 12; Andres et al., 2020). Therefore, given the lack of a significant decrease in velocities between Oleander and line W, except at 77 m, our interpretation is that the 77 m measurements described in Andres et al. (2020) may suffer from aliasing or other sampling issues. Furthermore, one does not expect the surface velocities at line W to significantly differ from the velocities at 77 m (difference on the order 10 cm max as discussed above), reinforcing the possibility that the observed 77 m measurements cannot be relied on. Andres et al. (2020) argue that small scale recirculation gyres are responsible or the differences, but this is not supported by the numerical experiments, nor by AVISO.

Furthermore, the line W measurements were collected during a 4-year period while the Oleander section benefits from a much longer time series. There is significant interannual variability in the north-south displacement of the main axis of the Gulf Stream at line W that may have contributed to the above-mentioned aliasing. Figures 10e, f displays the distribution of the SSH RMS (in cm) along the Oleander section and line W centered on the mean Gulf Stream path for the models and for two different AVISO time periods (1993–2022 and 2010-2014). First, one can note that the

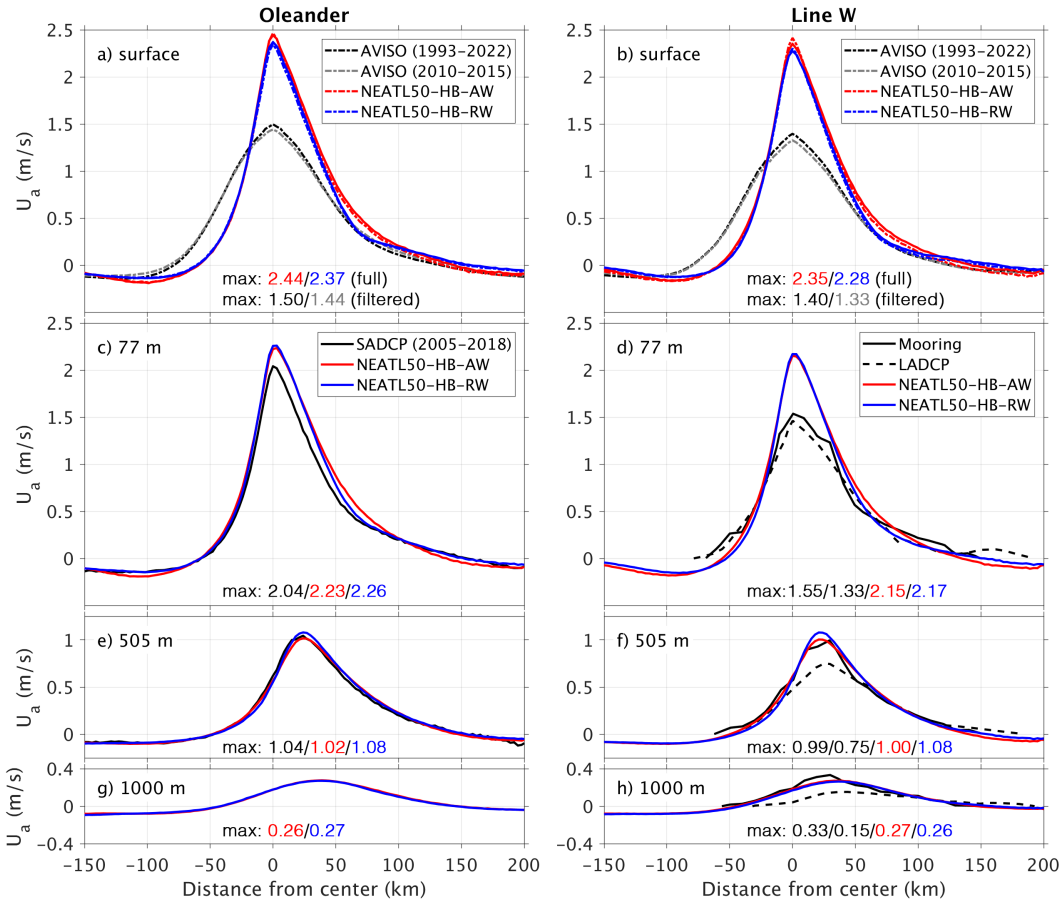

FIGURE 12
A comparison of the stream-averaged Gulf Stream jet between Oleander section (left) and line W (right) at **(a, b)** surface, **(c, d)** 77 m, **(e, f)** 500 m, and **(g, h)** 1000 m. In all panels, solid thick lines are total unfiltered velocities. In panels (a-b), dash doted lines are geostrophic velocities.

RMS distribution of the relative wind experiment (NEATL-HB-RW) is closer to the 1993–2022 AVISO-derived SSH RMS than the absolute wind experiment (NEATL-HB-AW), again showing the improvement in the representation of the Gulf Stream variability of using relative winds. There is, however, a significant difference in variability between the 2010–2014 and the 1993–2022 AVISO-derived SSH RMS. During 2010-2014, the SSH variability is smaller and narrower than during 1993–2022 at the Oleander section, but much larger and wider at line W. This does not translate in substantial differences on the core velocities (Figures 12a, b), but could lead to some aliasing at line W considering the sampling pattern (Andres et al., 2020).

The discussion above focused on the Oleander and W lines at 70.3°W and 68.5°W, respectively, and the question then arises as to how the numerical solutions compare upstream and downstream. Figure 3 does provide a broad picture of how the SSH variability varies along the Gulf Stream pathway in AVISO and the numerical experiments, but it does not give a quantitative measure of the variability of the meridional displacement of the jet. In Figure 14, we display the RMS of the north-south displacement of the Gulf Stream axis as a function of longitude. As one can anticipate from Figure 3, it is quite small (~50 km) until the Gulf Stream starts to "feel" the influence of the New England Seamount Chain around 65°W (Chassignet et al., 2023). On average, the relative wind experiment NEATL-HB-RW shows a north-south variability that is close to the observations (slightly less west of 60°W and more east of 50°W). The absolute wind experiment has significantly higher variability that observed east of 70°W (Figure 14), again demonstrating the importance of taking into account the ocean current feedback for a proper representation of the Gulf Stream variability as surmised by Renault et al. (2016).

3.4 Wavenumber power spectra

In the previous sections, we outlined the substantial differences in the Gulf Stream pathway and variability that arise from differences in wind stress formulation (relative versus absolute wind). Since the basin-wide kinetic energy has the same magnitude in both the absolute and the relative wind experiments (Figure 2), the differences in pathways and variability can only result from a redistribution of the sources and sinks of energy. The impact on ocean mesoscale variability of the current feedback on the atmosphere is well documented as it induces a damping of ~30%

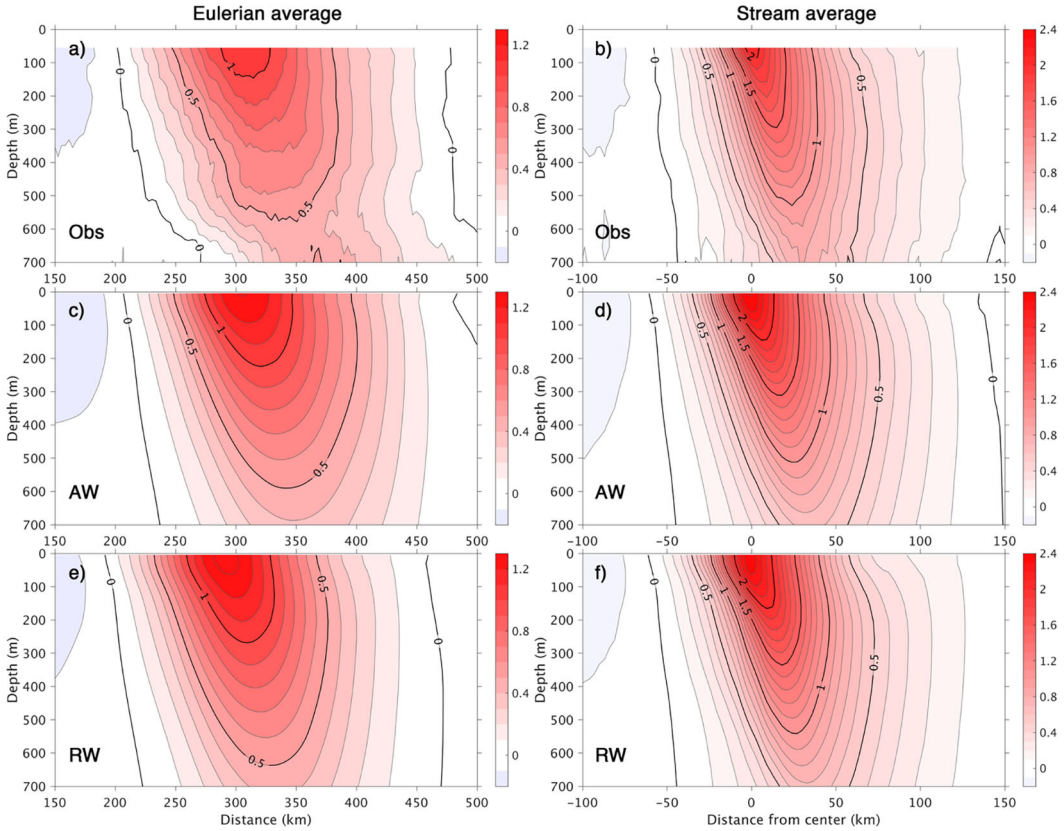

FIGURE 13
Comparison of Gulf Stream Eulerian and stream averages from **(a, b)** Oleander observations, **(c, d)** NEATL-HB-AW, and **(e, f)** NEATL50-HB-RW.

via a sink of kinetic energy to the atmosphere (Dewar and Flierl, 1987; Renault et al., 2016). The impact of the current feedback on the submesoscale is however not as strong, resulting in a more modest reduction of surface kinetic energy of ~10% (Renault et al., 2018, 2024). In this section, we use wavenumber spectra to quantify the impact of the current feedback on the 1/50° submesoscale-resolving North and Equatorial Atlantic simulations and to provide a measure of the energy and variability associated with different scales and regions.

Figure 15 shows the wavenumber spectra in SSH, kinetic energy, and relative vorticity for two 20° x 10° boxes: the highly energetic Gulf Stream (70°-50°W, 33°-43°N) and a more quiescent region in the eastern Atlantic (40°-20°W, 20°-30°N). As shown in Chassignet and Xu (2017), the SSH wavenumber spectra slopes in

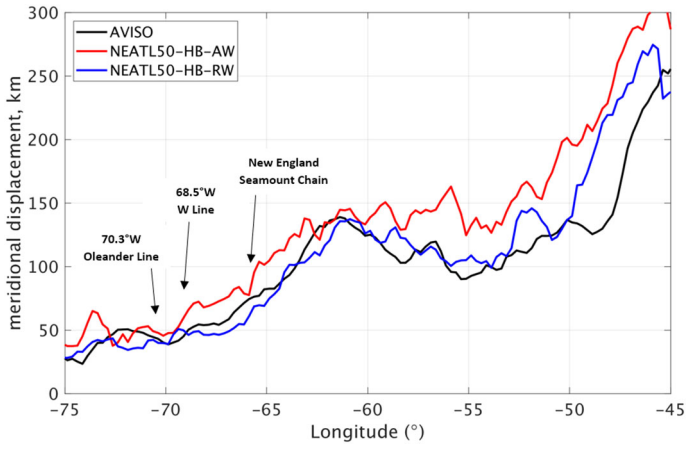

FIGURE 14
RMS of the north-south displacement of the Gulf Stream axis as a function of longitude.

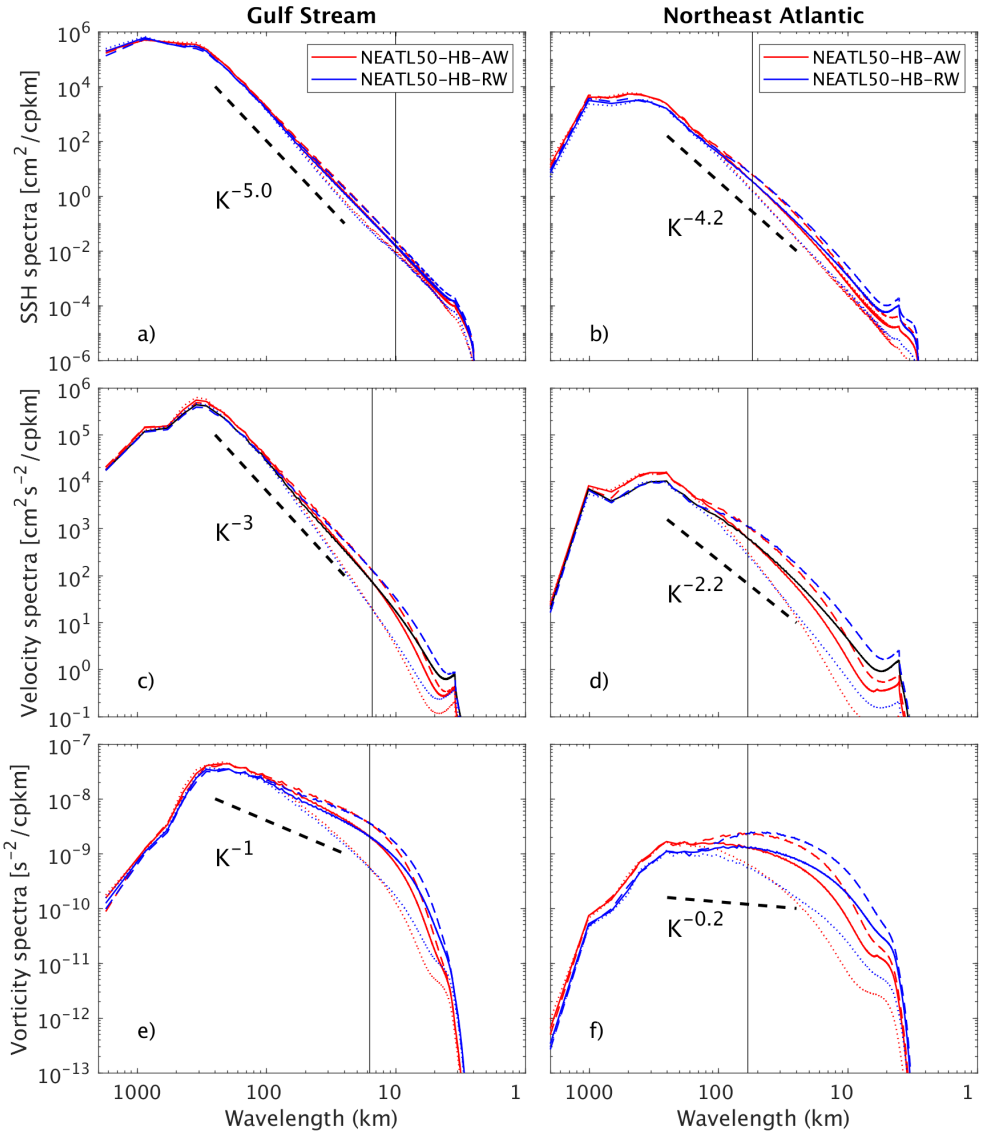

FIGURE 15
A comparison of wavenumber spectra of SSH **(a, b)**, surface velocity **(c, d)**, and surface relative vorticity **(e, f)** between the highly energetic Gulf Stream region (70°-50°W, 33°-43°N) and a less energetic region in the eastern Atlantic (40°-20°W, 20°-30°N). Annual, summer, and winter mean power spectra are denoted in solid, dotted and dashed lines, respectively.

the 70–250-km mesoscale range for both experiments is ~k$^{-4.2}$ for the low EKE region (SQG turbulence) and ~k^{-5} in the high EKE region (QG turbulence) (Wang et al., 2010). The slopes in the three wavenumber spectra do not differ much between NEATL-HB-AW and NEATL-HB-RW, but it is slightly steeper in NEATL-HB-AW which is a reflection of the fact that there is more energy in the large scales and less in the small scales when compared to NEATL-HB-AW. The scale separation between the two experiments is around 15 km in the high EKE Gulf Stream region and around 60 km in the low EKE interior region. This means that the current feedback is most effective at damping scales greater than 15–60 km (Figure 16) and that most of the energy loss in the large scales in NEATL-HB-RW (when compared to NEATL-HB-RW) is compensated by an energy increase in the submesoscale range, the latter being facilitated by the reduced horizontal viscosity (Table 2). This is further illustrated by Figure 16, which clearly shows the increase/decrease in submesoscale/mesoscale features in NEATL-HB-RW versus NEATL-HB-RW. There is a strong seasonality associated with enhanced submesoscale activity in the winter mixed layer (Mensa et al., 2013; Sasaki et al., 2014; Callies et al., 2015; Rocha et al., 2016). The biggest impact of the seasonal cycle is in the relative vorticity spectra (Figures 15e, f) with more energy in the smaller scales in the relative wind experiment.

4 Summary and conclusion

Current feedback affects time-dependent surface motions and the numerical experiments presented in this paper highlight its importance when modeling the Gulf Stream. This is not a new

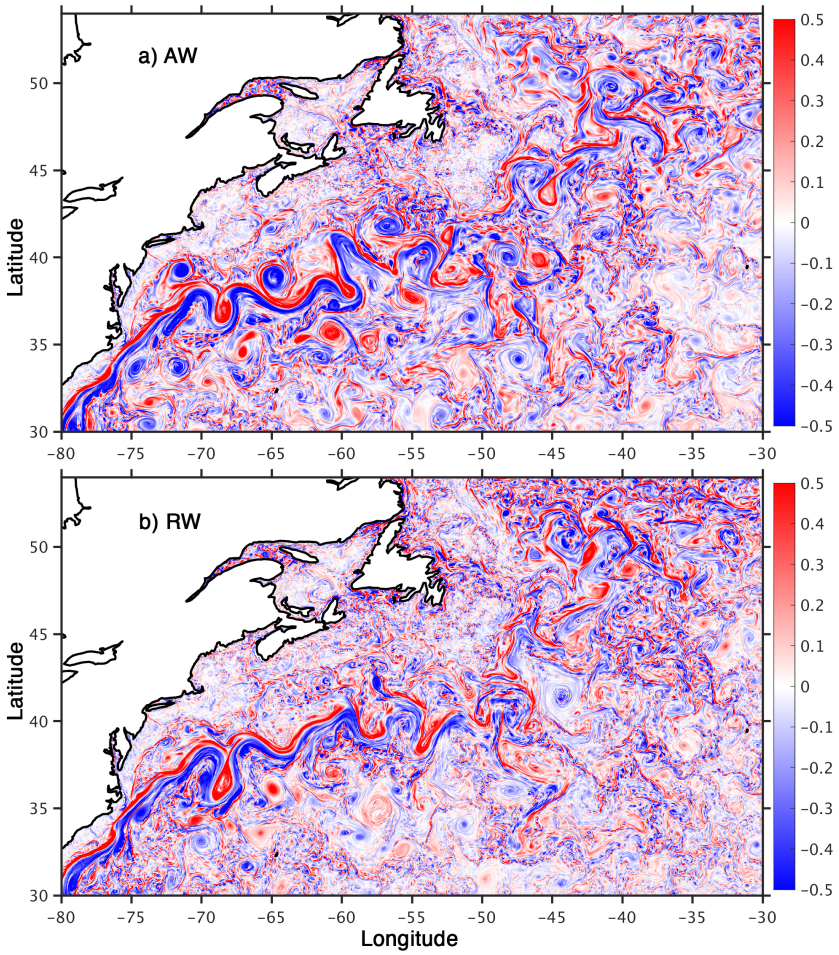

FIGURE 16
Snapshot of dimensionless surface relative vorticity (ζ/f with $f = 10^{-4}$ s^{-1}) in the Gulf Stream region on February 29 of year 20 for NEATL-HB-AW and NEATL-HB-RW, respectively. .

notion as the latter was already pointed out by Renault et al. (2016), but its implementation in the high-resolution 1/50° North and Equatorial Atlantic HYCOM domain of Chassignet et al. (2023) not only allows us to quantify its impact on the Gulf Stream pathway and variability via detailed comparisons to *in-situ* and altimetry data, but also to evaluate the latest mean dynamic topography derived from combining altimeter and satellite gravity data, drifters, and hydrological profiles (Jousset et al., 2025). Introduction of the current feedback does induce an "eddy-killing" effect that can reduce the level of eddy kinetic energy in the model by as much as 30%, but this drop in EKE can also be compensated by decreasing the model's explicit viscosity accordingly. As argued by Jullien et al. (2020), not considering the current feedback in a numerical model can lead to surface EKE levels as observed, but for the wrong reasons, i.e., by relying on numerical and explicit viscosity to compensate for the lack of an energy sink at the ocean's surface. The main difference between the absolute and the relative wind experiments discussed in this paper is in the redistribution of the sources and sink of energy. In the experiment with current feedback, the reduction in explicit viscosity leads to an increase in small-scale energy below 50–60 km while the current feedback is most effective at damping scales above that threshold. The current feedback is much less effective at damping submesoscale features (Renault et al., 2018, 2024).

Addition of the current feedback to the 1/50° North and Equatorial Atlantic HYCOM together with the viscosity/diffusivity reduction does lead to a much more realistic distribution of the sea surface height variability and the resulting mean field. A detailed comparison of the model results to altimeter data and *in-situ* measurements leads us to state that the Jousset et al. (2025) CNES-CLS22 mean dynamic topography underestimates the maximum Gulf Stream velocity by approximately 10%. An earlier version of the CNES-CLS MDT (CNES-CLS09) was compared by Worst et al. (2014) to *in-situ* data by integrating the ADCP velocities along the Oleander route and they found that CNES-CLS09 overestimated the sea surface height drop across the Gulf Stream (1.3 m versus 1.1m). The latest CNES-CLS22 MDT has a smaller total SSH change across the Gulf Strem than CNES-CLS09 which is more in line with the *in-situ* measurements. Another difference between the numerical and the latest observed MDT is in the circulation over the shelf region north of 40°N, i.e. none in the MDT. Either there are not enough observations to generate an

accurate MDT over the shelf, or the representation of the shelf circulation is incorrect in the model. A similar finding was reported by Chen and Yang (2024) as their high-resolution model also captures additional features that are missing from the CNES-CLS22 MDT, including the Labrador coastal current and a shelf break jet off the continental shelf of the US northeast, currents that has been verified in previous studies (e.g., Lazier and Wright, 1993; Loder et al., 1998).

Overall, we find an excellent agreement between the numerical model and the *in-situ* measurements, especially at depth. But, despite all the improvements in SSH mean and RMS, the model velocities are higher than observed at the surface. There are many factors that could be responsible for this difference, but we may still be missing a sink of energy as pointed out by Renault et al. (2023), i.e. the thermal feedback to the atmosphere. The thermal feedback is a consequence of the influence of the sea surface temperature on the atmosphere which modifies the turbulent heat flux and atmospheric boundary layer. As stated in Renault et al. (2023), the mesoscale thermal feedback causes heat flux anomalies that reduce the potential energy available in the ocean in favor of the atmosphere. Renault et al. (2024) emphasize the need to consider both thermal and current feedback together and that future parameterizations should be scale-aware and account for both thermal and current feedback effects on momentum and heat fluxes.

Data availability statement

The raw data supporting the conclusions of this article will be made available by the authors, without undue reservation.

Author contributions

EC: Writing – original draft, Writing – review & editing. XX: Writing – original draft, Writing – review & editing.

Funding

The author(s) declared that financial support was received for this work and/or its publication. Authors EC and XX were supported by the Office of Naval Research (Grant N00014-22-1-2574) and the NSF Physical Oceanography Program (Award 2241626). This work is a contribution to SWOT through the NASA Grants 80NSSC20K1135 and 80NSSC24K1649.

Acknowledgments

We thank Thomas Rossby for sharing the Oleander data and Kathleen Donohue, Nicholas Foukal, and Marco Larrañaga for constructive comments on an earlier version of this manuscript. The numerical simulations were performed on supercomputers at the Navy DoD Supercomputing Resource Center, Stennis Space Center, Mississippi, using computer time provided by the U.S. DoD High Performance Computing Modernization Program.

Conflict of interest

The author(s) declared that this work was conducted in the absence of any commercial or financial relationships that could be construed as a potential conflict of interest.

Generative AI statement

The author(s) declare that no Generative AI was used in the creation of this manuscript.

Any alternative text (alt text) provided alongside figures in this article has been generated by Frontiers with the support of artificial intelligence and reasonable efforts have been made to ensure accuracy, including review by the authors wherever possible. If you identify any issues, please contact us.

Publisher's note

References

Andres, M., Donohue, K. A., and Toole, J. M. (2020). The Gulf Stream's path and time-averaged velocity structure and transport at 68.5°W and 70.3°W. *Deep Sea Res.* 156, 103179. doi: 10.1016/j.dsr.2019.103179

Bleck, R. (2002). An oceanic general circulation model framed in hybrid isopycnic-Cartesian coordinates. *Ocean Model.* 37, 55–88. doi: 10.1016/S1463-5003(01)00012-9

Bleck, R., and Chassignet, E. P. (1994). "Simulating the oceanic circulation with isopycnic coordinate models," in *The Oceans: Physiochemical Dynamics and Resources* (Philadelphia: The Pennsylvania Academy of Science), 17–39.

Callies, J., Ferrari, R., Klymak, J. M., and Gula, J. (2015). Seasonality in submesoscale turbulence. *Nat. Commun.* 6, 6862. doi: 10.1038/ncomms7862

Carnes, M. R. (2009).Description and evaluation of GDEM-V3.0. *Naval Research Laboratory Memo*. Available online at: http://www7320.nrlssc.navy.mil/pubs/2009/carnes-2009.pdf (Accessed January 5, 2026).

Chassignet, E. P., and Garraffo, Z. D. (2001). "Viscosity parameterization and the Gulf Stream separation," in From Stirring to Mixing in a Stratified Ocean. Eds. P. Muller and D. Henderson. *Proceedings of the 12th 'Aha Huliko'a Hawaiian Winter Workshop. U. @ of Hawaii* (Hawaii, Honolulu) 37–41.

Chassignet, E. P., Hurlburt, H. E., Smedstad, O. M., Halliwell, G. R., Wallcraft, A. J., Metzger, E. J., et al. (2006). Generalized vertical coordinates for eddy-resolving global and coastal ocean forecasts. *Oceanography.* 19, 20–31. doi: 10.5670/oceanog.2006.95

Chassignet, E. P., and Marshall, D. P. (2008). "Gulf Stream separation in numerical ocean models," in *Ocean Modeling in an Eddying Regime*. Eds. M. Hecht and H. HasumiAGU Monograph Series (Washington, D.C.), 39–62. doi: 10.1029/177GM05

Chassignet, E. P., Smith, L. T., Halliwell, G. R., and Bleck, R. (2003). North Atlantic simulations with the hybrid coordinate ocean model (HYCOM): Impact of the vertical coordinate choice, reference pressure, and thermobaricity. *J. Phys. Oceanogr.* 33, 2504–2526. doi: 10.1175/1520-0485(2003)033<2504:NASWTH>2.0.CO;2

Chassignet, E. P., and Xu, X. (2017). Impact of horizontal resolution (1/12° to 1/50°) on Gulf Stream separation, penetration, and variability. *J. Phys. Oceanogr.* 47, 1999–2021. doi: 10.1175/JPO-D-17-0031.1

Chassignet, E. P., Xu, X., Bozec, A., and Uchida, T. (2023). Impact of the New England seamount chain on Gulf Stream pathway and variability. *J. Phys. Oceanogr.* 53, 1871–1886. doi: 10.1175/JPO-D-23-0008.1

Chassignet, E. P., Yeager, S. G., Fox-Kemper, B., Bozec, A., Castruccio, F., Danabasoglu, G., et al. (2020). Impact of horizontal resolution on global ocean-sea-ice model simulations based on the experimental protocols of the Ocean Model Intercomparison Project phase 2 (OMIP-2). *Geosci. Model. Dev.* 13, 4595–4637. doi: 10.5194/gmd-13-4595-2020

Chen, K., and Yang, J. (2024). What drives the mean along-shelf flow in the Northwest Atlantic coastal ocean? *J. Geophys. Res.: Oceans.* 129, e2024JC021079. doi: 10.1029/2024JC021079

Davis, T. J., Radko, T., Brown, J. M., and Dewar, W. K. (2025). Rough topography and fast baroclinic Rossby waves. *Geophys. Res. Lett.* 52, e2024GL112589. doi: 10.1029/2024GL112589

Dewar, W. K., and Flierl, G. R. (1987). Some effects of the wind on rings. *J. Phys. Oceanogr.* 17, 1653–1667. doi: 10.1175/1520-0485(1987)017<1653:Seotwo>2.0.Co;2

Halkin, D., and Rossby, H. T. (1985). The structure and transport of the Gulf Stream at 73°W. *J. Phys. Oceanogr.* 15, 1439–1452. doi: 10.1175/1520-0485(1985)015<1439:TSATOT>2.0.CO;2

Hurlburt, H. E., Metzger, E. J., Richman, J. G., Chassignet, E. P., Drillet, Y., Hecht, M. W., et al. (2011). "Dynamical evaluation of ocean models using the Gulf Stream as an example," in *Operational Oceanography in the 21st Century*. Eds. A. Schiller and G. Brassington (New York: Springer), 545–610.

Jousset, S., Mulet, S., Greiner, E., Wilkin, J., Vidar, L., Dibarboure, G., et al. (2025). New global mean dynamic topography CNES-CLS-22 combining drifters, hydrological profiles and high frequency radar data. *ESS Open Arch*. doi: 10.22541/essoar.170158328.85804859/v1

Jullien, S., Masson, S., Oerder, V., Samson, G., Colas, F., and Renault, L. (2020). Impact of ocean–atmosphere current feedback on ocean mesoscale activity: Regional variations and sensitivity to model resolution. *J. Climate.* 33, 2585–2602. doi: 10.1175/JCLI-D-19-0484.1

Large, W. G., McWilliams, J. C., and Doney, S. C. (1994). Ocean vertical mixing: A review and a model with a nonlocal boundary layer parameterization. *Rev. Geophys.* 32, 363–403. doi: 10.1029/94RG01872

Larrañaga, M., Renault, L., and Jouanno, J. (2022). Partial control of the Gulf of Mexico cynamics by the current feedback to the atmosphere. *J. Phys. Oceanogr.* 52, 2515–2530. doi: 10.1175/JPO-D-21-0271.1

Lazier, J. R. N., and Wright, D. G. (1993). Annual velocity variations in the Labrador current. *J. Phys. Oceanogr.* 23, 659–678. doi: 10.1175/1520-0485(1993)023<0659:avvitl>2.0.co;2

Loder, J. W., Petrie, B., and Gawarkiewicz, G. (1998). "The coastal ocean off northeastern North America: A large-scale view," in *The Sea* (New York City: John Wiley and Sons). Eds. A. R. Robinson and K. H. Brink, 105–133.

Mensa, J. A., Garraffo, Z., Griffa, A., Özgökmen, T. M., Haza, A., and Veneziani, M. (2013). Seasonality of the submesoscale dynamics in the Gulf Stream region. *Ocean Dyn.* 63, 923–941. doi: 10.1007/s10236-013-0633-1

Mulet, S., Rio, M.-H., Etienne, H., Artana, C., Cancet, M., Dibarboure, G., et al. (2021). The new CNES-CLS18 global mean dynamic topography. *Ocean Sci.* 17, 789–808. doi: 10.5194/os-17-789-2021

Paiva, A. M., Hargrove, J. T., Chassignet, E. P., and Bleck, R. (1999). Turbulent behavior of a fine mesh (1/12°) numerical simulation of the North Atlantic. *J. Mar. Sys.* 21, 307–320. doi: 10.1016/S0924-7963(99)00020-2

Renault, L., Contreras, M., Marchesielo, P., Conejero, C., Uchoa, I., and Wenegrat, J. (2024). Unraveling the impacts of submesoscale thermal and current feedbacks on the low-level winds and oceanic submesoscale currents. *J. Phys. Oceanogr.* 54, 2463. doi: 10.1175/JPO-D-24-0097.1

Renault, L., Masson, S., Arsouze, T., Madec, G., and McWilliams, J. C. (2020). Recipes for how to force oceanic model dynamics. *J. Adv. Model. Earth Syst.* 12, e2019MS001715. doi: 10.1029/2019MS001715

Renault, L., Masson, S., Oerder, V., Colas, F., and McWilliams, J. C. (2023). Modulation of the oceanic mesoscale activity by the mesoscale thermal feedback to the atmosphere. *J. Phys. Oceanogr.* 53, 1651–1667. doi: 10.1175/JPO-D-22-0256.1

Renault, L., McWilliams, J. C., and Gula, J. (2018). Dampening of submesoscale currents by air-sea stress coupling in the Californian upwelling system. *Sci. Rep.* 8, 13388. doi: 10.1038/s41598-018-31602-3

Renault, L., McWilliams, J. C., and Penven, P. (2017). Modulation of the Agulhas current retroflection and leakage by oceanic current interaction with the atmosphere in coupled simulations. *J. Phys. Oceanogr.* 47, 2077–2100. doi: 10.1175/JPO-D-16-0168.1

Renault, L., Molemaker, M. J., Gula, J., Masson, S., and McWilliams, J. C. (2016). Control and stabilization of the Gulf Stream by oceanic current interaction with the atmosphere. *J. Phys. Oceanogr.* 46, 3439–3453. doi: 10.1175/JPOD-16-0115.1

Rio, M. H., Guinehut, S., and Larnicol, G. (2011). New CNES-CLS09 global mean dynamic topography computed from the combination of GRACE data, altimetry, and in situ measurements. *J. Geophys. Res.: Oceans.* 116, C07018. doi: 10.1029/2010JC006505

Rio, M.-H., and Hernandez, F. (2004). A mean dynamic topography computed over the world ocean from altimetry, in *situ* measurements, and a geoid model. *J. Geophys. Res.: Oceans.* 109, C12032. doi: 10.1029/2003JC002226

Rio, M.-H., Mulet, S., and Picot, N. (2014). Beyond GOCE for the ocean circulation estimate: synergetic use of altimetry, gravimetry, and in *situ* data provides new insight into geostrophic and Ekman currents. *Geophys. Res. Lett.* 41, 8918–8925. doi: 10.1002/2014GL061773

Rocha, C. B., Gille, S. T., Chereskin, T. K., and Menemenlis, D. (2016). Seasonality of submesoscale dynamics in the Kuroshio Extension. *Geophys. Res. Lett.* 43, 11304–11311. doi: 10.1002/2016GL071349

Rossby, T., Andres, M., Chafik, L., and Donohue, K. (2025). A comparative study of velocity and transport estimates along the Oleander line between Bermuda and New Jersey. *Earth Space Sci.* 12, e2024EA004090. doi: 10.1029/2024EA004090

Rossby, T., Flagg, C. N., Donohue, K., Fontana, S., Curry, R., Andres, M., et al. (2019). Oleander is more than a flower: Twenty-five years of oceanography aboard a merchant vessel. *Oceanography.* 32, 126–137. doi: 10.5670/oceanog.2019.319

Samelson, R. M., Durski, S. M., Chelton, D. B., Skyllingstad, E. D., and Barbour, P. L. (2024). Surface currents and relative-wind stress in coupled ocean-atmosphere simulations of the northern California Current System. *Mon. Wea. Rev.* 152, 2033–2054. doi: 10.1175/MWR-D-23-0279.1

Sasaki, H., Klein, P., Qiu, B., and Sasai, Y. (2014). Impact of oceanic-scale interactions on the seasonal modulation of ocean dynamics by the atmosphere. *Nat. Commun.* 5, 5636. doi: 10.1038/ncomms6636

Smith, W. H. F., and Sandwell, D. T. (1997). Global sea floor topography from satellite altimetry and ship depth soundings. *Science.* 277, 1956–1962. doi: 10.1126/science.277.5334.1956

Teague, W. J., Carron, M. J., and Hogan, P. J. (1990). A comparison between the generalized digital environmental model and Levitus climatologies. *J. Geophys. Res.* 95, 148–227. doi: 10.1029/89JC03682

Uppala, S. M., KÅllberg, P. W., Simmons, A. J., Andrae, U., Da Costa Bechtold, V., Fiorino, M., et al. (2005). The ERA-40 re-Analysis. *Quart. J. R. Meteor. Soc.* 131, 2961–3012. doi: 10.1256/qj.04.176

Wang, D., Flagg, C. N., Donohue, K., and Rossby, H. T. (2010). Wavenumber spectrum in the Gulf Stream from shipboard ADCP observations and comparison with altimetry measurements. *J. Phys. Oceanogr.* 40, 840–844. doi: 10.1175/2009JPO4330.1

Worst, J. S., Donohue, K. A., and Rossby, T. (2014). A Comparison of vessel-mounted acoustic doppler current profiler and satellite altimeter estimates of sea surface height and transports between New Jersey and Bermuda along the CMV Oleander Route. *J. Atmos. Oceanic Technol.* 31, 1422–1433. doi: 10.1175/JTECH-D-13-00122.1